Effects of Large and Spread Explosives Loads

Bibiana Luccioni[1,3] +, Daniel Ambrosini[2,3], Steeve Chung Kim Yuen[4], Gerald Nurick[4]

[1]Structures Institute, National University of Tucumán, Tucumán, Argentina
[2]Structural Engineering Master Program. Eng. Faculty. Nat. Univ. of Cuyo, Mendoza, Argentina
[3]CONICET, National Research Council from Argentina, Buenos Aires, Argentina
[4]Blast Impact and Survivability Research Unit (BISRU), Department of Mechanical Engineering, University of Cape Town, South Africa

ABSTRACT

This paper presents experimental data and numerical analysis of the effects of detonating explosive charges ranging from 1000 to 26288 kg laid out on the ground. The charges consist of different ordnances widespread in a carpet-like form. Numerical analysis using ANSYS/Autodyn are carried out with a view to gain a better understanding of the blast loading resulting from the detonation of large masses of ordnance. Good correlation between the numerical results and experiments in terms of crater dimensions and blast wave parameters is obtained. The influence of the charge configurations on the blast wave parameters and crater shape are also investigated. While the cube root scaled distance works well for the evaluation of pressure and impulse values produced by a relatively compact charge layout, the scaled distance parameter has to be modified for cases where charges are spread in a carpet-like fashion.

Keywords: large explosions, soil, crater, blast wave, numerical model.

1. INTRODUCTION

Explosive devices are available in different sizes. Table 1 lists the suggested classification for explosive devices, in four main groupings based on the size of the charge, by Nurick et al. [1]. Category S1 is a device of mass up to 0.1 kg of TNT that enables indoor laboratory blast testing. Category S2 (0.1-10 kg TNT) consists of devices that require outdoor laboratory experimentation. The explosive devices in the medium (M: 10-100 kg TNT), large (L: 100-1000kg TNT) and extreme (E: >1000kg TNT) categories consist of different size weapon-type systems.

+Corresponding author. Tel.: +54-381-364087; fax: +54-381-364087 E-mail address: bluccioni@herrera.unt.edu.ar

Table 1. Categorization of size of explosive devices (1).

Category	SMALL		MEDIUM	LARGE	EXTREME
	S1	S2	M	L	E
Facilities	Indoor Laboratory	Outdoor Laboratory /Test Range	Test Range	Test Range	Test Range
Mass	Up to 0.1 Kg	>0.1 Kg to 10Kg	>10 Kg to 100Kg	>100Kg to 1000Kg	>1000Kg
Example	Hand grenade Antipersonnel Mine	Land-Mine Portable Mines	Torpedo Air Bomb	War Head	Oklahoma Nuclear bomb
References	[3-6]	[7-9]	[10-11]		[12-13]

Whilst numerous different tests investigating the response of soils and structures, such as beams and plates, to blast loading conditions in the S1 category have been published in the open literature, reports describing structural response using medium to extreme explosive devices are limited or classified [2].

Ambrosini et al[14] reported on a series of tests performed with different amounts of explosive at short distances above and below ground level, as well as on soil surface and presented a numerical study on craters formed by explosive loads located on soil surface[15]. The soil parameters used in the numerical model, as well as the analysis procedure, were validated against experimental observations of the crater diameters. Moreover, the effect of elevation of the centre of energy release of explosive loads located on the soil surface were analyzed and discussed. Simple predictive equations for the crater diameter were presented. In a recent paper, the accuracy of numerical simulations, using a hydrocode, of craters produced by underground explosions was demonstrated [16]. Several numerical approaches were carried out using different constitutive models and processors for the soil. In order to validate the numerical approach and demonstrate its ability to model the crater formation, comparison with experimental results was performed. Many simulations of the same physical model lead to the same crater dimensions and a good agreement between the test results and the predicted crater measures was achieved. Recently, a study investigating craters created by exploding charges ranging from 120 kg to 1900 kg of TNT was presented [17]. The charge consists of different ordnances stacked in different configurations corresponding to tests performed at Touwsrivier Training Range (South Africa) [13]. The arrangement of the explosive load was shown to have significant importance in the final dimensions of the crater.

Empirical equations for the evaluation of blast wave parameters can be found in the specialized literature. However, these equations have been obtained for spherical explosives. Moreover, these formulae are based on scaling laws that were proved to work well for that shape of explosives. In other studies concerning blast load assessment and the effect of blast loads on structures spherical explosives of no more than 1000 kg of TNT were used [18].

Recently, Yuen et al. [2] presented the results of two test programmes in which quadrangular mild steel plates were subjected to pressure loads created by exploding charges ranging from 100 to 26,288 kg in mass. The charge consisted of different ordnances stacked in different configurations, namely compacted and widespread in a carpet-like form. The effect of the charge configurations on the response of the square mild steel plates was investigated. Simple analytical evaluations of the pressures and impulses were used for the purpose of comparison with the experiments. The correlation shows satisfactory agreement, despite the imperfect terrain and different complex explosive loading arrangement. This

paper presents the experimental data and numerical simulation of the different craters generated by the different blasts. The test programme was performed at the Vastrap Weapons Range, South Africa [2] with explosive loads in the extreme category (equivalent TNT masses of explosive greater than 1000 kg). The charge consists of different ordnances widespread in a carpet-like form. Numerical results are compared with experimental results of crater dimensions. The effects of the charge configurations and mass of explosive on the crater dimensions and shape are investigated and empirical formulae are proposed. The blast wave generated and the effect on steel plates is also numerically studied and the results are compared with those obtained in the experiment [2].

2. THEORY AND PREVIOUS RESULTS
INTRODUCTION
Historically, the analysis of explosions has predominantly involved simplified analytical methods [19-21]. Nowadays empirical formulae obtained from numerical and experimental studies are still very useful to perform quick prediction of the response of soils and structures to blast load. A brief description of the empirical formulae that are later compared with experimental and numerical results of craters dimensions, blast wave parameters and plate deflections is presented in this section.

CRATER FORMATION
Most of the information about explosively formed craters found in the literature is based on experimental data. Tests of crater formation are appropriate tools to study the blast phenomena, the behavior and destructive power of different explosives, and the response of soils and rocks under this type of load [22]. The mechanism of crater formation is complex and is related to the dynamic physical properties of air, soil, and soil-air interface. Even very carefully performed cratering tests give deviations in the dimensions measured of the order of 10%, while differences of as much as 30% to 40% are common [23].

A cavity is always formed when an explosion is produced on a mass of soil. The crater dimensions defined by Kinney and Graham [20], used in this paper, are illustrated in Fig. 1; D is the apparent crater diameter and H is the apparent depth of the crater.
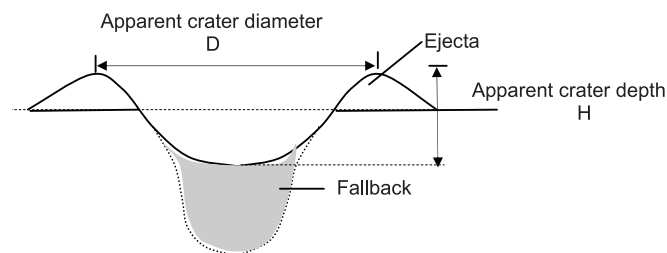

Figure 1. Definitions of the crater dimensions.

The most important variables in defining the crater shape and size are the mass W of the explosive and the location of the explosive with respect to the ground. Studies concerned with the characteristics of craters caused by explosions usually resort to dimensional analysis and statistics. The scaling law establishes that any linear dimension L of the crater can be

expressed as a constant multiplied by W^α divided by the distance of the charge from the ground, where α is a coefficient that is dependent on whether the gravitational effects can be neglected or not. When the gravitational effects can be neglected the cubic root law is applicable $\alpha = 0.33$ and in the other cases the functional dependence can be quite complex. Henrych [24] presents many empirical and semiempirical formulae so as a theoretical calculation of crater parameters that take into account soil properties. All of them are related to craters produced by underground explosions. There is not much information about explosions at ground level. Statistical studies of about 200 accidental above-ground explosions of relatively large magnitude are presented by Kinney and Graham [20]. The results exhibit a variation coefficient in the crater diameter of about 30%. From these results, the empirical Eqn. (1) for the crater diameter was proposed [20],

$$D(m) = 0.8W^{1/3}(kg) \pm 30\% \qquad (1)$$

Ambrosini et al[14] have conducted a series of tests with different amounts (1-10 kg of TNT) of explosive at short distances above and below ground level, as well as on the soil surface. The explosive load was spherical in all tests. The numerical study on craters formed by explosive loads located on the soil surface was also presented [15]. From these results, the Eqn. (2) was proposed for the evaluation of the apparent diameter of the crater formed by spherical blast loads laid on the ground,

$$D(m) = 0.51W^{1/3}(kg) \pm 5\% \qquad (2)$$

The variation of ±5% accounts for the differences between soil properties that could be found in different sites.

In connection with the morphological and structural types of the craters, Melosh [25] determines four different basic types: (a) bowl-shaped, (b) flat-floored with central uplift, (c) flat floored with a peak ring, and (d) flat floored with more than two asymmetric rings (multi-ring basins). Numerical and independent research presented by Iturrioz et al. [26] confirms preliminarily the formation of the same shapes of craters. In all these studies the variable analyzed is the height of burst that defines the diameter to height ratio of the crater.

Generally, all these studies were performed with compact explosives: spherical, cylindrical, cubic, etc and explosive charges up to the medium range (less than 100 kg of TNT). Previous numerical results obtained by Luccioni et al. [16] show that there is no difference in the craters produced by compact explosive loads of different shapes. There is, however, no information in open literature related to crater shape produced by large and spread explosives.

BLAST LOAD PARAMETERS

The most widely used approach for blast wave scaling is Hopkinson's law [19] which establishes that similar explosive waves are produced at identical scaled distances when two different charges of the same explosive and with the same geometry are detonated in the same atmosphere. Thus, any distance R from an explosive charge W can be transformed into a characteristic scaled distance Z, given by Eqn. (3)

$$Z = R / W^{1/3} \qquad (3)$$

where W is the charge mass expressed in kilograms of TNT and R the distance from the

explosive in meters. The corresponding masses for other explosives can be obtained through the concept of TNT equivalence [9]. The use of Z allows a compact and efficient representation of blast wave data for a wide range of situations.

There are many solutions for the wave front parameters produced by spherical explosives from both numerical simulations and experimental measurements [19-21]. The results are usually presented in graphics, tables or equations based on experimental or numerical results, such as the Eqn. (4) presented by Kinney and Graham [20],

$$\frac{p_S}{p_o} = \frac{808\left[1+(Z/4.5)^2\right]}{\sqrt{1+(Z/0.048)^2}\,\sqrt{1+(Z/0.32)^2}\,\sqrt{1+(Z/1.35)^2}} \tag{4}$$

where t is the time, p_o is the ambient pressure, p_s is the peak overpressure.

The accuracy of predictions and measurements in the near field is lower than in the far field, probably due to the complexity of blast phenomena [21]. This observation is particularly important for large explosions where even large stand off distances give small scaled distances, see Eqn. (3).

The side-on specific impulse i_s represents the area under the overpressure time history. Results of specific impulse produced by free field spherical explosives are usually given in tables and graphics as a function of the scaled distance [19-21]. For a quick evaluation of the specific impulse value, the negative phase of the typical pressure–time history of a blast load [7] can be neglected and a triangular pulse can be assumed.

EFFECT OF BLAST LOAD ON STEEL PLATES

It has been widely demonstrated that the effect of blast loads on structures can be mainly attributed to impulse and the structures properties, that is, geometry, materials and supports (boundary conditions). Dimensionless analysis provides a useful insight into scaling to enable a better understanding of the characteristic response of geometrically similar plates subjected to impulsive loading. Nurick and Martin [4,5] reported on a dimensionless impulse ϕ_q, Eqn. (5), for quadrangular plates subjected to uniform blast load

$$\phi_q = \frac{I}{2h^2(BL\rho\sigma_o)^{0.5}} \tag{5}$$

where I is the total impulse; B the plate breadth; L the plate length; h the plate thickness; ρ the material density and σ_o the material static yield stress.

Considering a uniform blast load, the total impulse can be obtained as, Eqn. (6):

$$I = i_s\,(BL) = i_s A \tag{6}$$

where A represents the plate exposed area.

Nurick and Martin [4,5] also presented an empirical relationship, Eqn. (7), to predict the mid-point deflection– thickness ratio of thin quadrangular plates subjected to uniform blast load using the dimensionless number given in Eqn. (7).

$$\frac{\delta}{h} = 0.48\phi_q \tag{7}$$

where δ is the mid-point deflection.

The repeatability confidence envelope for Eqn. (7) is reported as 90% for 1 plate thickness and 99% for 2 plate thicknesses, for plate thickness of 1.6mm, [27].

Using Eqns. (5) and (7), the mid-point deflection a quadrangular plate is calculated as, Eqn. (8)

$$\delta = \frac{0.48I}{2h(BL\rho\sigma_o)^{0.5}} \qquad (8)$$

It should be noted that this empirical relationship was developed from experiments, (in category S1), where the charge and plate response are carried out in a controlled set-up and shown to apply for bigger blast loads [1,2].

3. EXPERIMENTAL PROGRAMME

The tests were conducted on the Vastrap Weapons Range located 1000 km north west of Cape Town, a vast test area, which is fairly flat and sandy. Because of its vast area each test was carried out on a different location on the range leaving the crater resulting from the blast untouched. 11 blast tests with explosive masses ranging from 500 to 26,288 kg were performed. The blasts were created using ordnance such as Projectile AS MK 10, Warhead KC5, Warhead KC9, 84mm HE and 90mm HE shells. Each test comprised a stack of ammunition as required to configure the predetermined mass. The list of test is presented in Table 2. All the explosive masses are converted into TNT equivalent. For the Minol Explosives, as used in AS MK 10, the TNT equivalent mass is 1.2M. For the Amatol Explosives, as used in the KC5/KC9, the TNT equivalent mass is 0.95M. For the cyclotol explosives, as used in the HE shells, the TNT equivalent mass is 1.1M [28,29].The ordnance was laid out in a carpet-like way on the flat ground in different stacking pattern to provide the most favourable packing –labour –time layout. A typical charge lay-out is shown in Fig. 2(a) (Test 10). The dimensions of the explosive in plan are indicated in Fig.3 and presented in Table 2.

Figure 2: Blast test 10. a) Explosive layout; b) Steel plate

Figure 2. Blast test 10. a) Explosive layout; b) Steel plate

For almost all the tests, the dimensions of the craters produced by the explosive loads were measured as indicated in Fig.3 and presented in Table 2. Three or four (grey (G), red (R), blue (B), yellow(Y)) quadrangular mild steel plates of 3 and 6mm thick were placed at different distances from the explosives loads in each blast test. A plate-clamping station, 700x700 mm^2 (Fig.2b) in size, was used to provide the quadrangular specimen with suitable support to enable the pressure loadings to result in large inelastic deformations of the exposed area of 500 x 500 mm^2. The entire

Table 2. Vastrap tests (2)

N°	Ammunition	Charge Kg	Equiv. TNT mass W kg	Explosive Layout		Plate thick. h (mm)	Stand off dist. R (m)	Meass. deflec δ (mm)	Crater dimensions (m)		
				a(m)	b(m)				A	B	H
1	Anti-tank shells 90mm	1018	1119.8	5.0	8.7	6	18.50	0.0	8.7	10.8	0.8
						3	18.00	5.0			
						3	22.50	2.5			
						3	19.50	4.2			
2	Anti-tank shells 90mm	1032	1135.2	7.3	9.2	6	8.80	14.7	----	----	----
						3	13.35	28.6			
						3	12.25	37.3			
						3	8.65	40.7			
3	Anti-tank shells 90mm	2046	2250.6	5.4	9.4	3	13.30	35.5	10.3	12.0	0.9
						3	15.00	33.1			
						6	11.30	37.3			
						3	18.60	22.0			
4	Anti-tank shells 90mm ASMK10 (x10)	3268	3694.8	2.3	11.8	3	18.20	36.8	10.7	18.7	1.8
						6	16.20	18.1			
						3	27.90	12.8			
						3	20.70	34.7			
5	Anti-tank shells 84mm	6314	6945.4	2.7	17.3	6	21.25	0.0	11.0	23.0	2.2
						3	24.65	7.4			
						3	25.45	0.0			
						3	20.95	7.9			
6	Anti-tank shells 90mm ASMK10 (x10)	2996	3395.6	2.3	11.6	3	21.00	9.1	17.0	22.2	2.3
						6	14.50	45.2			
						3	18.00	35.5			
						3	16.00	50.2			
7	Anti-tank shells 84mm	12020	13222	3.4	13.3	6	19.30	4.2	15.3	21.6	----
						3	27.20	15.7			
						3	22.85	10.4			
						3	19.20	27.8			
8	Anti-tank shells 84mm ASMK10 (x10)	19959	22054.9	4.5	16.3	3	26.60	34.8	15.0	25.5	2.7
						3	24.90	31.8			
						3	20.20	60.6			
9	ASMK10 (x5)	500	600	1.2	1.25	3	14.80	23.0	8.1	8.1	2.5
10	Anti-tank shells 84 and 90mm	25063	27569.3	9.2	16.5	6	17.00	70.2	20.2	27.2	3.0
						3	20.80	103.0			
						3	24.00	50.9			
						3	20.40	202.0			
11	ASMK10 (x90), KC5 (x18) KC9 (x41)	26288	27223.6			6	22.30	70.3	-----	-----	-----
						3	25.50	83.0			

plate support system was fixed to the ground. The stations were positioned so that the plate faces the ordnance. The station set-up configuration is shown in Fig. 2(b).The mid point deflections of all the plates were recorded and listed in Table 2. The damage due to shrapnel was neglected as it was localised and not considered significant to cause global plate response [2]. For full details of the blast tests see Yuen et al.[2].
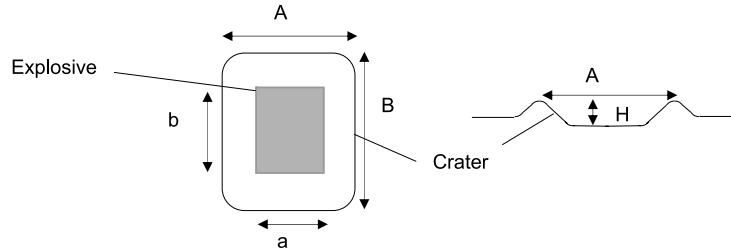
Figure 3. Explosive and crater sketch

4. NUMERICAL MODELS

INTRODUCTION

All the numerical analysis is performed with the hydrocode ANSYS/Autodyn[30]. In order to carry out a comparable analysis, the mass of the explosive is defined by TNT masses. The corresponding masses for other explosives can be obtained through the concept of TNT equivalence.

An Euler Godunov multi material with strength higher order processor [31] is used to model the problems including the air, the explosive charge and the soil. The steel plates are modelled with shell elements and interaction with the Euler mesh is defined.

MATERIAL MODELS

The ideal gas equation of state is used for the air. Lee-Tarver equation of state [32] is used to model both the detonation and expansion of TNT in conjunction with "Jones -Wilkins - Lee" (JWL EOS) to model the unreacted explosive.

A shock Eqn. [33] of state is used for the soil. The initial density is taken as $\rho = 2.2$ g/cm^3 (wet density). The wet density is obtained considering a mean dry density of 2100 kg/m^3 and a moisture content of 5%.

It has been experimentally proved that for most solids and many liquids there is a linear relationship between the shock velocity U and the material velocity behind the shock u_p over a wide range of pressure,

$$U = c_o + su_p \tag{9}$$

Where c_o is sound speed.

The Mie-Gruneisen form of equation of state based on the shock Hugoniot is used,

$$p = p_h + \Gamma\rho(e - e_h) \tag{10}$$

Where e is the internal energy, ρ is the density and Γ. is the Gruneisen Gamma, defined as,

$$\Gamma = v\left(\frac{\partial p}{\partial v}\right)_v \tag{11}$$

p is the pressure and v the specific volume.
It is assumed that $\Gamma\rho = \Gamma_o\rho_o$ = constant and

$$p_h = \frac{\rho_o c_o^2 \mu (1+\mu)}{[1-(s-1)\mu]^2} \quad e_h = \frac{1}{2}\frac{p_h}{p_o}\left(\frac{\mu}{1+\mu}\right) \tag{11}$$

where $\mu = \dfrac{\rho}{\rho_o} - 1$

The assumption of constant $\Gamma\rho$ is probably not valid. Furthermore, the assumption of a linear variation between the shock velocity U and the particle velocity u_p does not hold for too large compression pressure. At high shock strengths some nonlinearity in this relationship is apparent, particularly for non-metallic materials. This non linearity can be covered by a smooth interpolation between two linear relationships or by a quadratic shock velocity [33].

An elastoplastic strength model based on Drucker Prager criterion and a hydro tensile limit are also used for the soil. The yield stress is a piecewise linear function of pressure. A summary of properties used for soil is presented in Table 3.

In recent papers, the accuracy of numerical simulations of craters produced by explosions on the soil surface [15] and underground explosions was proved [16], [34]. Although the blast wave generated in soil is strongly dependent on soil model and properties [34], elastic properties, failure limit and yield function of the soil do not significantly affect the diameter of the crater obtained [15], [16].

A linear equation of state combined with a Johnson and Cook model [30] for strength is used for mild steel plates. The material properties are presented in Table 4.

BOUNDARY CONDITIONS

In order to fulfil the radiation condition, a transmitting boundary is defined for soil subgrids external limits. The transmitting boundary condition allows a stress wave to continue "through" the physical boundary of the subgrid without reflection. The transmit boundary is only active for flow out of a grid. Air and TNT flow through grid sides is also allowed over the ground level. The size of the numerical mesh can be reduced using this type of boundary condition. Nevertheless, the boundaries should not be close to the crater because the transmit boundary is only an approximation and some spurious wave reflections could be expected to take place on boundaries.

Table 3. Soil properties

Equation of State: Shock	Strength: Drucker Prager	
Reference density $\rho = 2.2$ g/cm^3	Shear Modulus $G = 2.4\ 10^5$ kPa	
Gruneisen Gamma $\Gamma = 0.11$	Pressure 1 $=-1.149\ 10^3$ kPa	Yield stress 1 = 0 kPa
$c_o = 1.614\ 10^3$ m/s	Pressure 2 = $6.88\ 10^3$ kPa	Yield stress 2 = $6.2\ 10^3$ kPa
$S = 1.5$	Pressure 3 = $1.0\ 10^{10}$ kPa	Yield stress 3 = $6.2\ 10^3$ kPa
	Hydro tensile limit $p_{min} = -100$ kPa	

Table 4: Mild steel properties

Equation of State: Linear	Strength: Johnson Cook
Reference density $\rho = 7.8$ g/cm^3	Shear Modulus $G = 8.18 \ 10^7$ kPa
Bulk Modulus K=1.59 10^8kPa	Yield Strength 2.5 10^5 kPa
	Hardening Constant 5.1 10^5 kPa
	Hardening Exponent 0.26
	Strain Rate Constant 0.014

5. CRATER FORMATION

INTRODUCTION

The simulation of craters produced by explosive loads widespread in a carpet-like form is presented in this section. First the blast tests described in section 3 are numerically reproduced and the results are compared with experimental ones. Further numerical analysis is carried out in order to study the effects of the charge configurations and mass of explosive on the crater dimensions.

NUMERICAL SIMULATION OF VAPSTRAP TESTS

Tests covering the range of 600 to 27569.3 kg of equivalent TNT masses are numerically simulated. These tests correspond to blast tests in Table 2 for which the crater dimensions have been obtained. Using symmetry conditions, only a quarter of the problem is simulated. The charge layouts with its associated numerical models used are presented in Fig. 4. The dimensions of the models are indicated on Fig.4. In each model soil, air and TNT are modelled. For clarity, air is not represented in the models shown in Fig.4. The explosive is widespread in the same area as in the experiment. In the case of tests 1 and 3, three explosive strips are modelled to represent the experiments. The mesh is refined in coincidence with the explosive load to have at least ten cells within the explosive in each direction [30]. A detail of the mesh refinement for test 8 is presented in Fig.5. Detonation lines are defined in correspondence with detonators in each test. The simulation is carried out until the craters remain unchanged.

a)

a) Test 1 (1119.8 kg equivalent TNT);

b)

b) Test 3 (2250.8 kg equivalent TNT;
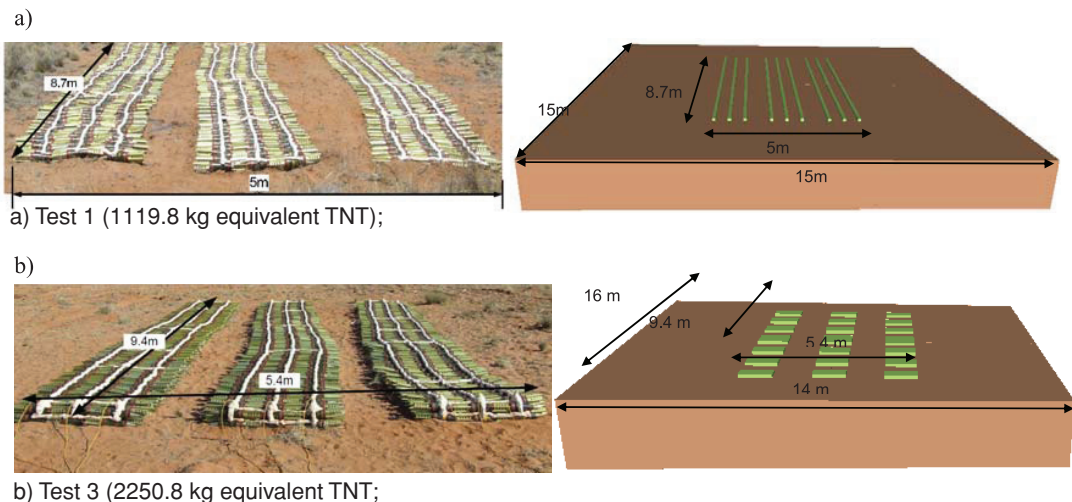
Figure 4.

c)
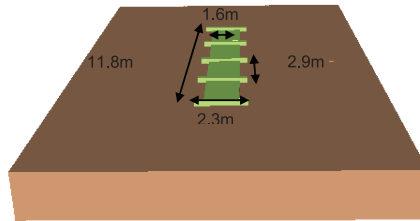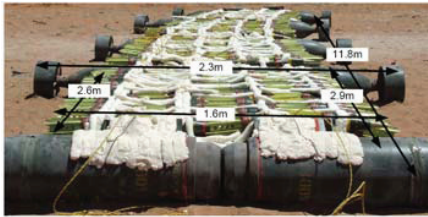
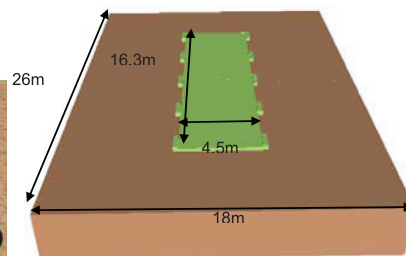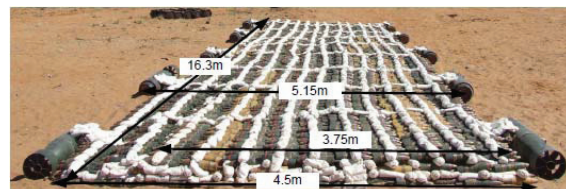c) Test 4 (3694.84 kg equivalent TNT);

d)
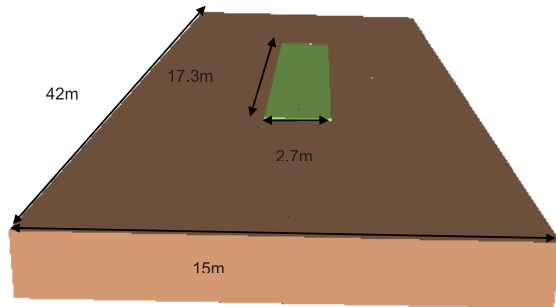
d) Test 5 (6945.4 kg equivalent TNT);

e)
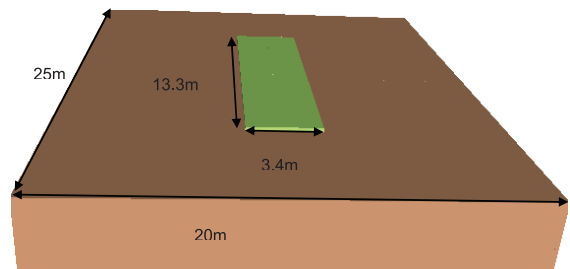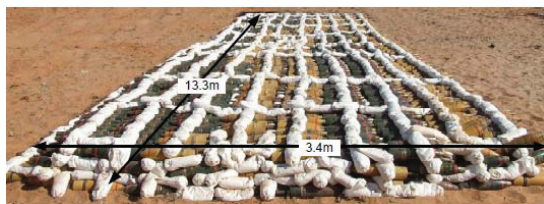
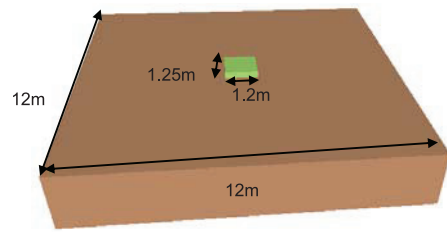e) Test 7 (13222 kg equivalent TNT);

f)

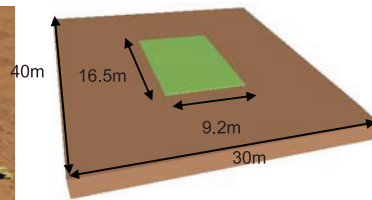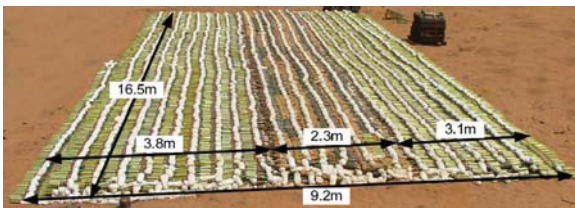

f) Test 8 (22054.9 kg equivalent TNT);

Figure 4. (continued)

g)

g) Test 9 (600 kg equivalent TNT);

h)

h) Test 10 (27569.3 kg equivalent TNT)
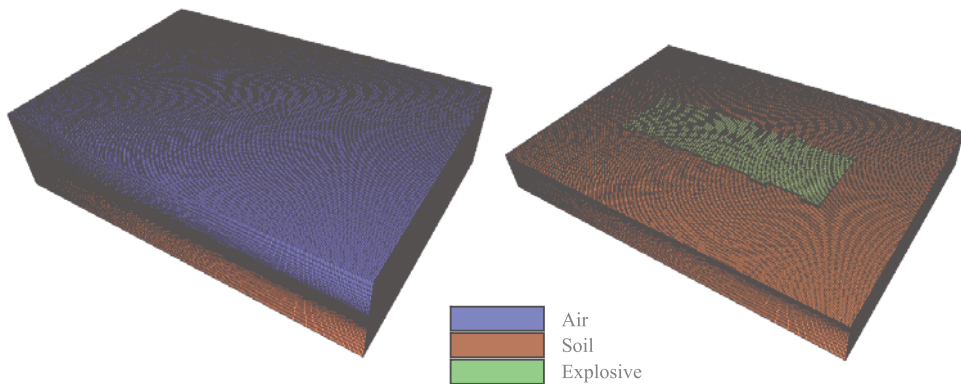
Figure 4. Numerical models for Vastrap tests.

Air
Soil
Explosive

Figure 5. Numerical models details for Vastrap Test 8 (22054.9 kg equivalent TNT);

Figs.6 to 13 show the comparison of craters produced by the explosive tests and those obtained with the numerical models. The numerical results for the crater dimensions are presented in Table 5 and compared with experimental dimensions presented in Table 2. There is a reasonable agreement between numerical and experimental results in all cases. The differences are in the order of the variability in experimental measures for this type of tests. The craters simulated are always smaller and more stretched than actual craters and a good agreement in crater depth indicated as H in Fig. 3 is achieved. The biggest difference corresponds to blast test 6. The stack of ammunition used in this test was similar to that of blast test 4 so numerical results are identical in both cases. The differences observed in experimental craters could be attributed to the different "linked explosives" used (PE4 in blast test 4 and elephant powergel explosives in blast test 6)

Table 5. Crater dimensions

Tests No.	Fig.	W kg TNT	Crater width		Crater length		Crater height	
			A(m)	Dif %	B(m)	Dif %	H(m)	Dif %
1	6	1119.8	6.3	27.6	10.6	1.6	0.7	16.0
3	7	2250.8	7.5	27.0	11.2	6.7	1.0	-11.1
4	8	3694.8	4.6	57.0	15.0	24.7	1.9	-5.5
5	9	6945.4	8.2	25.	22.6	1.7	2.5	-13.6
6	8	3395.6	4.6	72.9	15.0	31.8	1.9	-17.4
7	10	13222.0	9.6	37.3	18.8	13.0	----	----
8	11	22054.9	9.2	38.7	19.4	23.9	1.7	37.0
9	12	600.0	5.6	30.0	5.6	30.0	2.9	-16.0
10	13	27569.3	15.8	21.8	23.0	15.4	3.3	-10.0

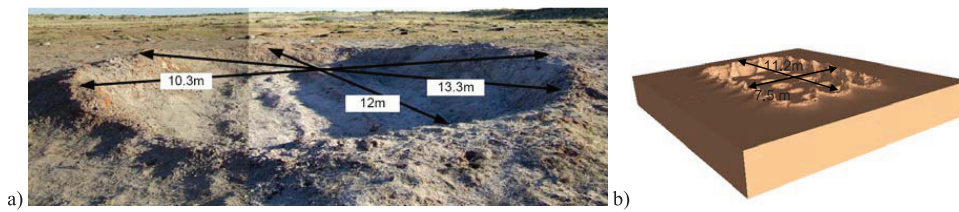Figure 6. Crater obtained for Test 1 (1119.8 kg equivalent TNT): a) Experimental; b) Numerical

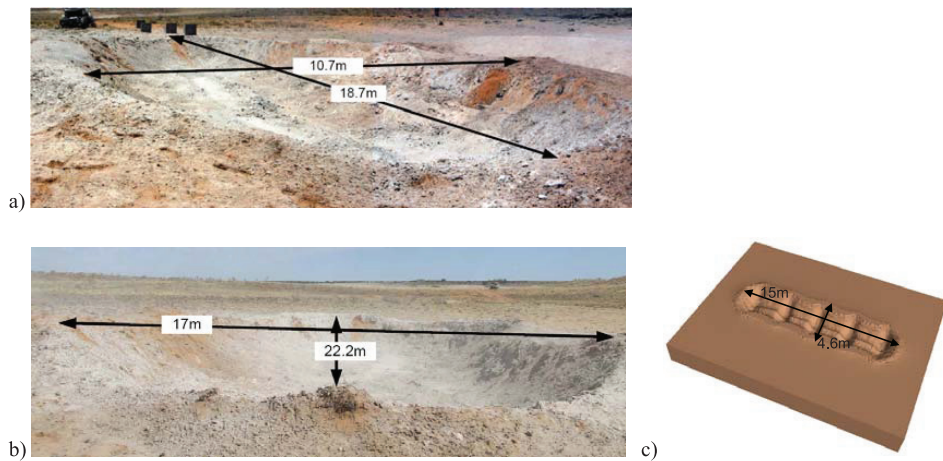Figure 7. Crater obtained for Test 3 (2250.8 kg equivalent TNT): a) Experimental; b) Numerical

Figure 8. Crater obtained for Tests 4 and 6 (3694.8-3395.6 kg equivalent TNT):a) Experimental test 4; b) Experimental test6; c) Numerical
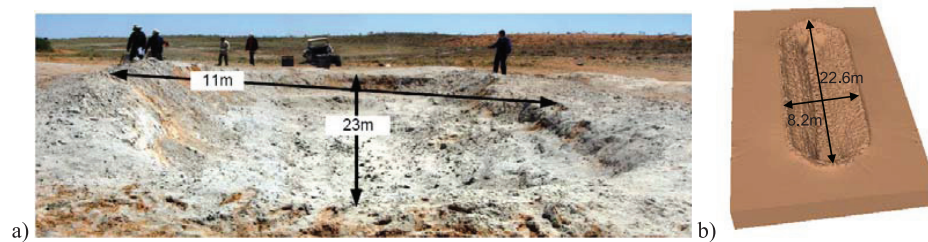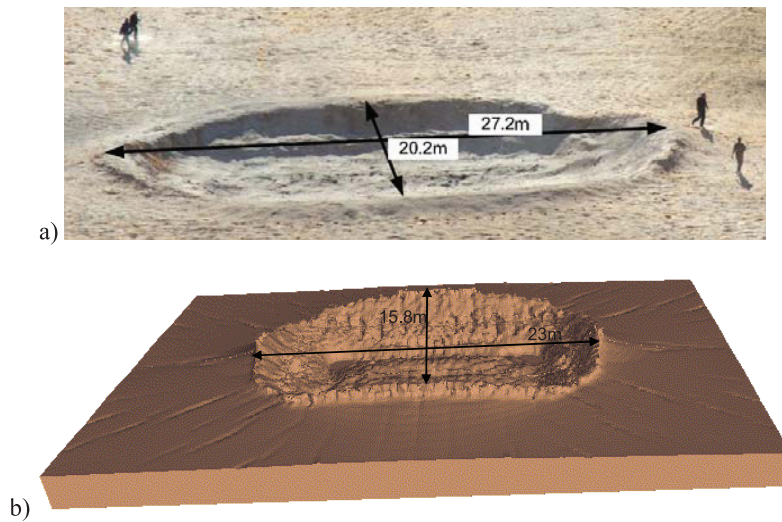

Figure 9. Crater obtained for Test 5 (6945.4 kg equivalent TNT): a) Experimental; b) Numerical

Figure 10. Crater obtained for Test 7 (13222 kg equivalent TNT): a) Experimental; b) Numerical

Figure 11. Crater obtained for Test 8 (22054.9 kg equivalent TNT): a) Experimental; b) Numerical

Figure 12. Crater obtained for Test 9: a) Experimental; b) Numerical

Figure 13. Crater obtained for Test 10 (27569.3 kg equivalent TNT): a) Experimental; b) Numerical
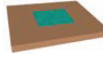
ANALYSIS OF THE EFFECT OF EXPLOSIVE LAYOUT ON THE DIMENSIONS AND SHAPE OF THE CRATERS

In order to study the effect of explosive charge layout on crater dimensions, the craters produced by the same explosive charges of three blast tests but with different explosive shapes are simulated. The explosive masses are chosen to cover a range from 1119.8 to 27569.3 kg equivalent TNT. Two different layouts are modelled for each explosive mass: (C) a cylindrical carpet-like layout with the same area in plan as the tests and (M) a cylindrical compact layout with diameter equal to height.

In order to study the effect of plan shape of explosive layout on crater shape, a square carpet-like explosion (S) of 27569.3 kg equivalent TNT with the same area as in test 10 is additionally modelled. Due to symmetry conditions, cylindrical problems are simulated with axi-symmetric models with a considerable save in computational time in comparison with actual shape numerical tests presented in section 3. Circular detonation lines with the same spacing in plan as in rectangular tests are defined for the case of cylindrical numerical models.

The diameters of the craters obtained are presented in Table 6 for comparison with experimental and numerical equivalent diameter (diameter of the circle with equal area) of the craters produced by actual shape explosives. It can be seen that the equivalent diameter of craters produced by cylindrical explosive loads is always smaller than that obtained for the rectangular layout used in the tests. Moreover, when the explosive is concentrated in a compact cylinder (M), even smaller craters are obtained. As the aspect ratio (b/a) of the explosive increases, the area of the crater and thus the equivalent diameter are greater.

Table 6. Crater diameters for different explosive layouts

W (kg equivalent TNT)	Rectangular layout Equivalent crater diameter D (m)		Cylindrical layout Crater diameter D (m)		Square Carpet-like Crater diameter D (m)
	Experiment	Numerical	Numerical carpet-like explosive (C)	Numerical-Compact explosive (M)	Numerical (S)
1119.8	10.9	9.2	8.4	6.0	–--
6945.4	17.9	15.4	11.8	8.5	–--
27569.3	26.4	21.5	18.4	11.1	16.6

ANALYSIS OF RESULTS

All the results obtained in previous sections are plotted on Fig.14 representing the equivalent apparent crater diameter as a function of the cubic root of the equivalent TNT explosive mass. The lines corresponding to Eqns (1) and (2) with the inferior and superior bounds together with points corresponding to experimental and numerical results previously obtained by Ambrosini et al [14,15,17] are also plotted in Fig.14. The points correspond to experimental results from crater tests with spherical explosive loads of 1-10 kg TNT lying on the ground [14], numerical crater tests with spherical explosive loads of 50-500 kg TNT lying on the ground [15] and numerical crater tests for compact (not cylindrical) explosive charge layouts of 120-1900 kg TNT reported by Ambrosini and Luccioni [17].

The tendency remarked in previous section relating craters produced by different explosive layouts is clear in Fig.14. While craters produced by carpet-like explosives are better represented by Eqn. (1), crater diameters obtained for compact explosives are better represented by Eqn. (2). In both cases, it seems that the linear approximation is only valid for explosive loads up to the large category (L) (less than 1000 kg TNT). In order to represent the complete range of explosive masses simulated, the Eqns (9) and (10) are proposed for carpet-like explosives and compact explosives respectively.

$$(C) \quad D(m) = 1.929 W^{1/4} \tag{12}$$

$$(M) \quad D(m) = 0.834 W^{1/4} \tag{13}$$

Eqns (12) and (13) are represented in Fig.15 together with experimental and numerical results. A good agreement with experimental and numerical results for all the equivalent TNT explosive mass range studied (0-27569.3 kg TNT) is obtained using the new linear approximation with $W^{1/4}$ instead of $W^{1/3}$.
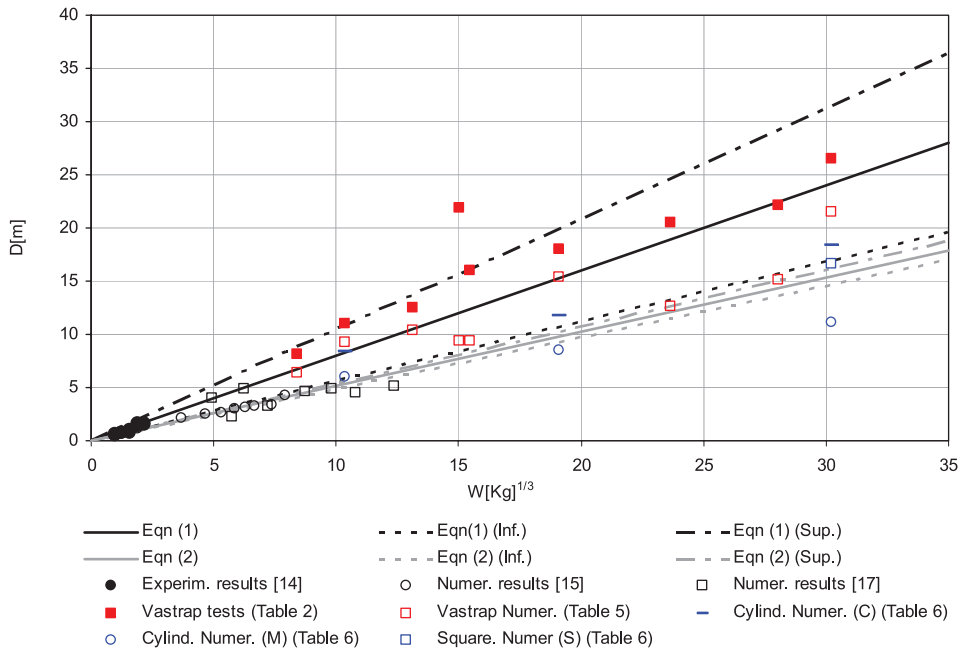
Figure 14. Apparent crater diameter produced by explosive loads located on the ground
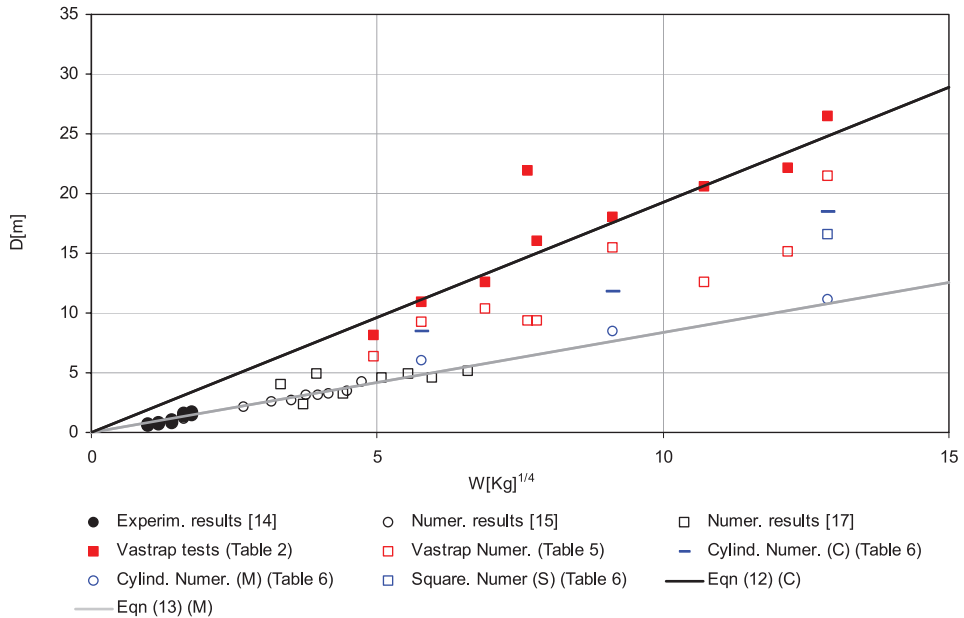

Figure 15. Proposed relationship for apparent crater diameter for explosive load on the ground

Experimental and numerical apparent crater depth values are plotted as a function of $W^{1/4}$ in Fig.16. Experimental and numerical results previously obtained by Ambrosini et al [14,17] are also plotted in Fig.16. The crater depth obtained with compact explosives is always greater than that obtained with carpet-like explosives. A linear relation between apparent crater depth and $W^{1/4}$ cannot be clearly established in this case.
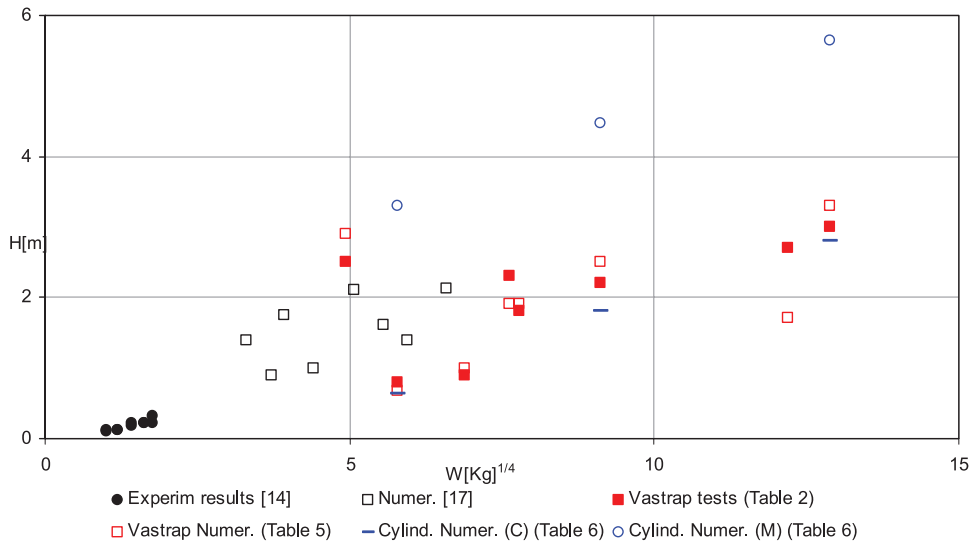

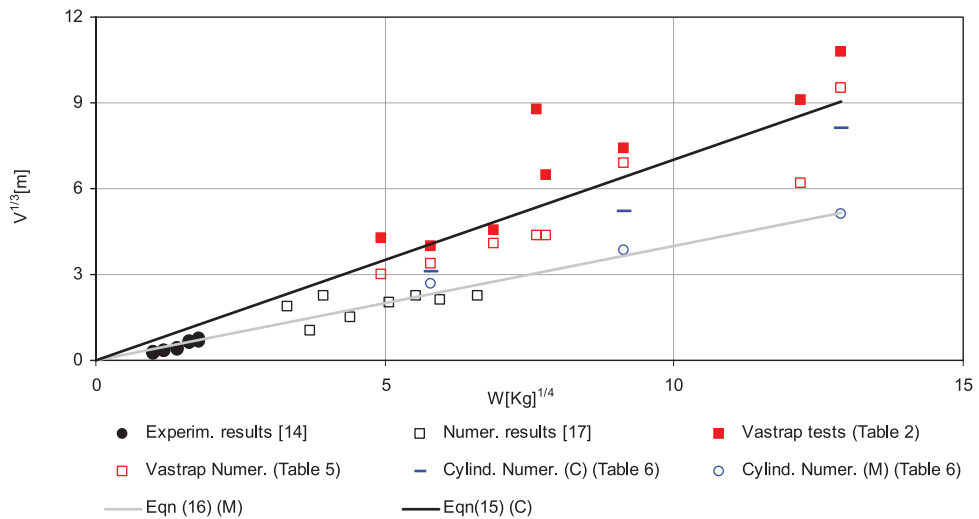Figure 16. Apparent crater depth produced by explosive loads located on the ground

Figure 17. Apparent crater volume produced by explosive loads located on the ground

Experimental and numerical apparent crater volume cubic root values are plotted as a function of $W^{1/4}$ in Fig.18. Apparent crater volume is calculated approximately as follows,

$$V = (A - H)(B - H)H \qquad (14)$$

Experimental and numerical results previously obtained by Ambrosini et al [14,17] are included in Fig.17. The crater volume obtained with compact explosives is always smaller than that obtained with carpet-like explosives. A linear relation between apparent crater volume cubic root $V^{1/3}$ and $W^{1/4}$ can be established through Eqns. (15) and (16) for carpet-like explosives and compact explosives respectively.

$$(C) \qquad V^{1/3}(m) = 0.701W^{1/4} \qquad (15)$$

$$(M) \qquad V^{1/3}(m) = 0.399W^{1/4} \qquad (16)$$

6. BLAST WAVE PARAMETERS AND PLATE DEFLECTIONS
INTRODUCTION
In order to assess the parameters of the blast wave originated from different explosive layouts, the pressure and impulse time history at points situated at different distances from the explosive charge center are registered for all the cylindrical blast tests simulated. The gauge points are located at a height of 350mm in coincidence with the mid-points of the steel plates. Some gauge points are also located in the numerical models of Vastrap tests 5 and 10. These points are coincident with some of the steel plates in the tests. Two mild steel plates are also simulated in test 10. As stated in Ref [18], blast wave parameters obtained from numerical tests are strongly dependent on mesh size. In order to minimize this type of error, the mesh was refined until the same results were obtained. A 25 mm mesh in each direction was used.

BLAST WAVE PARAMETERS
The resulting peak overpressure values as a function of the scaled distance are represented in Fig.18a. Distances are measured from the explosive center. For the cases of cylindrical explosives, the same models are run but avoiding blast wave reflection on the ground. The corresponding results are also plotted on Figs.18. In this way, the effect of ground reflection can be evaluated. From Fig.18a, it can be concluded that the effect of blast wave reflections on the ground is important in the case of compact explosives but it is almost negligible in case of widespread explosives. The difference observed can be attributed to the shape of the wave front originated in both explosive layouts.

The curve corresponding to empirical Eqn. (3) is also included in Fig.18a. The comparison with numerical results shows that while the cubic scale law works well for free field compact explosions, it is not appropriate for carpet-like explosions. For carpet like explosives overpressure values are smaller than those predicted by empirical Eqn. (3). Following the results presented in Ref. [2], a modified scaled distance is proposed as Eqn. (17)

$$Z' = R / W^{1/4} \quad [m/kg^{1/4}] \qquad (17)$$

Peak overpressure values obtained for the carpet-like explosives are represented as a function of Z' in Fig.18b. The resulting points are almost coincident with the empirical curve corresponding pressure evaluated using Eqn. (3) but for Z' instead of Z.
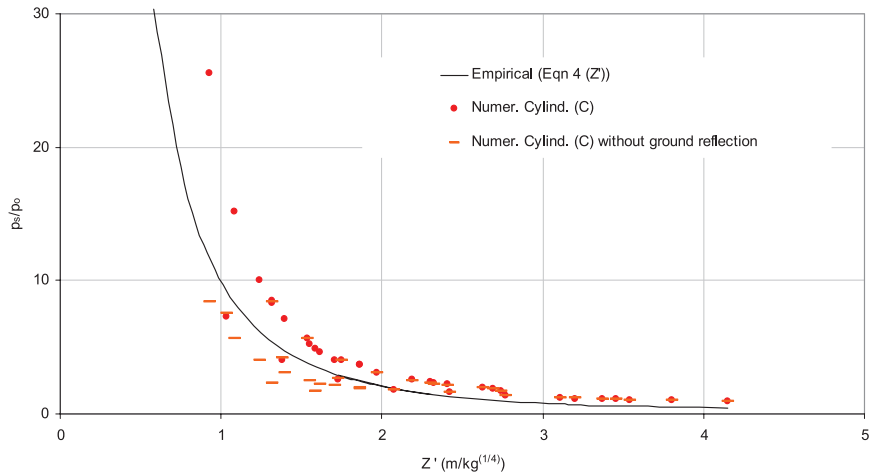
a)
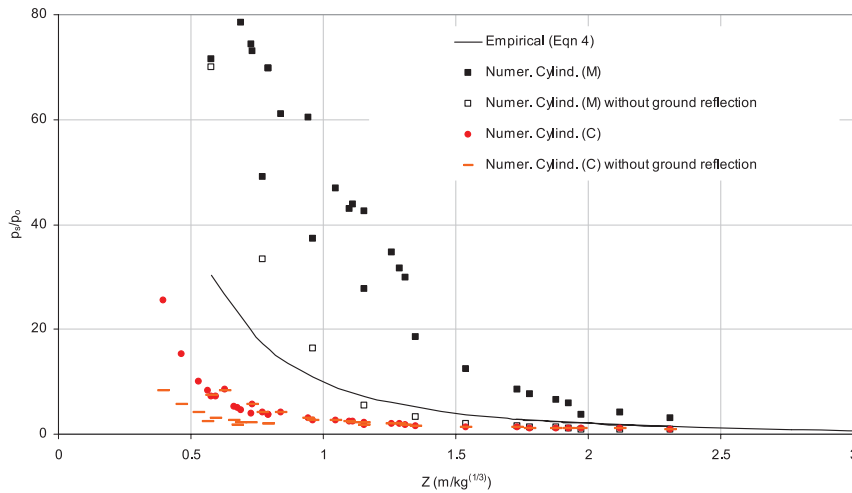
b)

Figure 18. Peak side on overpressure. (a) Scaled distance Z, (b) Modified scaled distance Z'

The peak specific impulse values as a function of the scaled distance are represented in Fig.19a. Like in the case of overpressure values, the impulse values for compact blast loads are greater than those for carpet like explosives.

Nevertheless, the tendency of results is not so clear like in the case of overpressure values. Impulse values for compact explosive loads follow with some scattering the empirical curve presented by Kinney and Graham [20]. Points corresponding to impulse values are closer to

that curve when they are represented as a function of the modified scaled distance Z' defined by Eqn. (17) in Fig. 19b but, despite empirical results, they tend to a constant value, even greater than that predicted by empirical equations for high scaled distances ($Z' > 3$). It can be seen that for this explosive charge, numerical impulse values are lower than empirical values for $Z' < 2.5$.
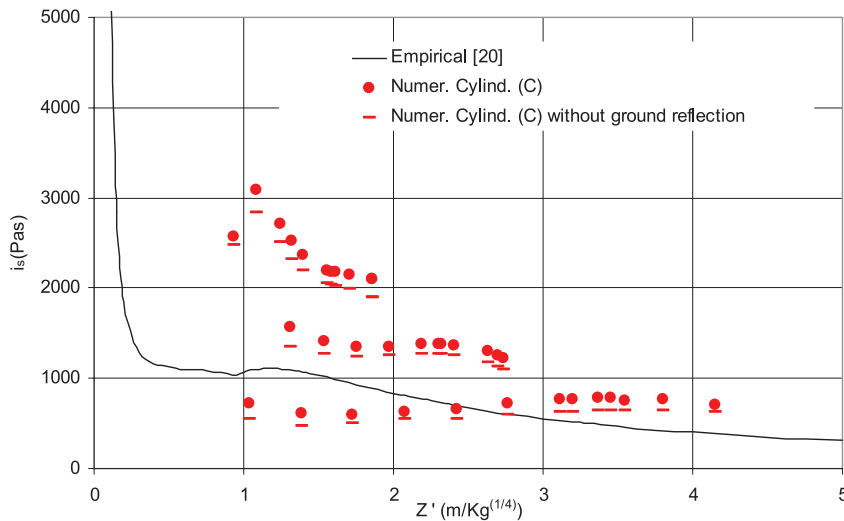
a)
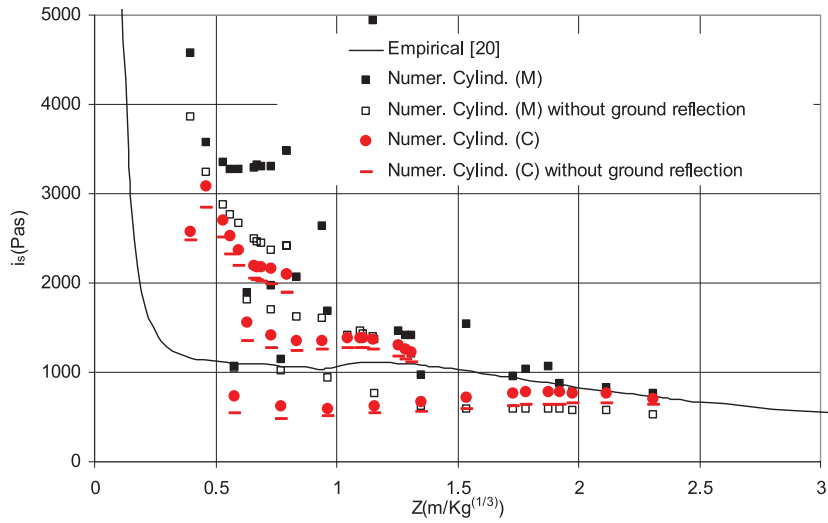
b)

Figure 19. Peak side on impulse vs modified scaled distance. (a) Scaled distance Z, (b) Modified scaled distance Z'

PLATE DEFLECTIONS

With the impulse values empirically [20] and numerically obtained, the plates maximum permanent deflections can be estimated using Eqns. (6) and (8). From this relationship, the mid-point deflection of a 500x500 mm steel plate (static yield stress = 250MPa, density = 7850 kg/m^3) can be calculated as [2],

$$\delta \text{ [mm]} = 0.114\text{I [N s]} \quad \text{for plate thickness 3mm} \tag{18}$$
$$\delta \text{ [mm]} = 0.057\text{I [N s]} \quad \text{for plate thickness 6mm} \tag{19}$$

Numerical values of impulse are directly obtained from the different models. Empirical values are calculated using the modified scaled distance Z'. The corresponding mid-point deflection values are represented in Fig.20 as a function of the modified scaled distance together with the measured values of mid-point deflection for both plate thicknesses tested (3 and 6 mm). Experimental results are also plotted on Fig.20. In all cases, greater plate deflections are predicted for concentrated (M) than for carpet like explosives (C). Empirical results lie close to those corresponding to carpet-like explosive layout simulated.

Although numerical points are not coincident with experimental results, they follow the same tendency. The result suggests good correlation within a maximum of six plate thicknesses It seems that the use of Z' combined with Eqn. (8) works better for higher scaled distances than for lower scaled distances. For small scaled distances (greater blast loads) registered deflections are much greater than calculated deflections.

In order to analyze the origin of the differences observed, a steel plate corresponding to test 10 is included in blast model shown in Fig.4h. Shell elements of the actual shell thickness are used and the annular clamps are also included in the model as thicker parts of the plate. 14 by 14 elements of 50 mm by 50 mm side are used for the steel plate. The plate is clamped at the base and at the upper corners to simulate the support shown in Fig.2b. Figure 21a shows the deformation of a 6mm plate located at 17m from the centre of the explosive load. It can be seen that the deformed pattern corresponds to a uniform pressure. Figure 21b shows the midpoint displacement as a function of time. The plate deflects and then vibrates with a permanent deflection. The maximum permanent deflections obtained for the plate is included in Fig 20b (Red squares: Numer.). The maximum permanent deflection is closed to that obtained in the test and greater than that previously calculated using numerical impulse value obtained for a cylindrical carpet like explosive and Eqn. (8) (Numer.(C)).

7. CONCLUSIONS

The numerical results presented in this paper provide an insight into the effect of large-scale explosions. The loading condition resulting from the detonation of large amount of ordnance widespread on the ground in a carpet like fashion has proven to be different from that produced by the detonation of compact explosives.

Reasonable agreement of numerical results with the experiment was obtained for crater dimensions. The shape and the dimensions of the crater formed in the underlying soil strongly depend on the explosive layout. The equivalent crater diameter for carpet like explosives is always greater than that for compact explosives. Moreover, for carpet like explosives, the equivalent diameter is greater for rectangular layouts than for circular layouts. It was also demonstrated that existing empirical formula for the prediction of crater diameter are not adequate for explosive masses greater than 3500 kg and new expressions covering all the range of explosives masses, from small to extreme cases, are proposed.

While the cube root scaled distance works well for evaluating the pressure and impulse values originated from a compact charge layout, the scaled distance parameter has to be modified to a fourth root for cases where charges are spread in a carpet-like fashion. The effect of blast wave reflections on the ground is almost negligible for this type of explosive layout.
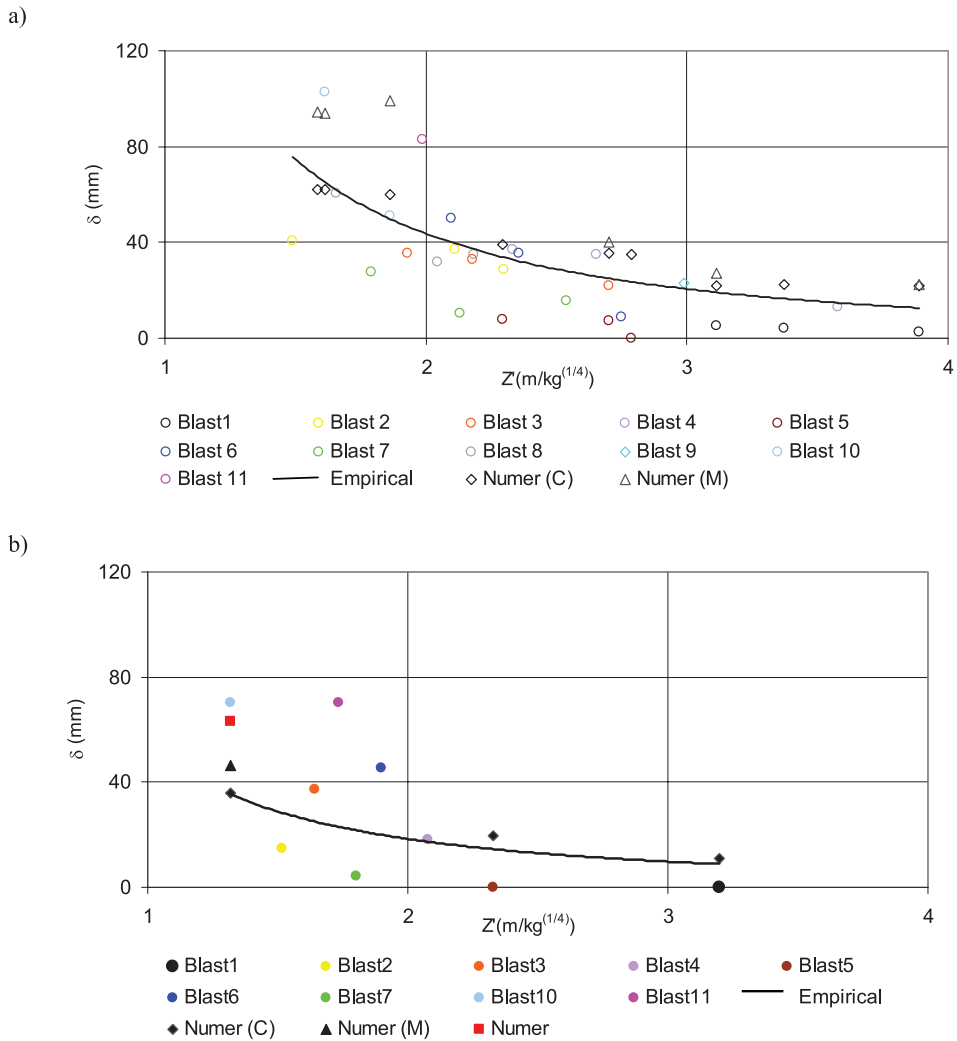
a)

b)

Figure 20. Plates mid point deflection. a) 3mm thickness plate, b) 6mm thickness plate
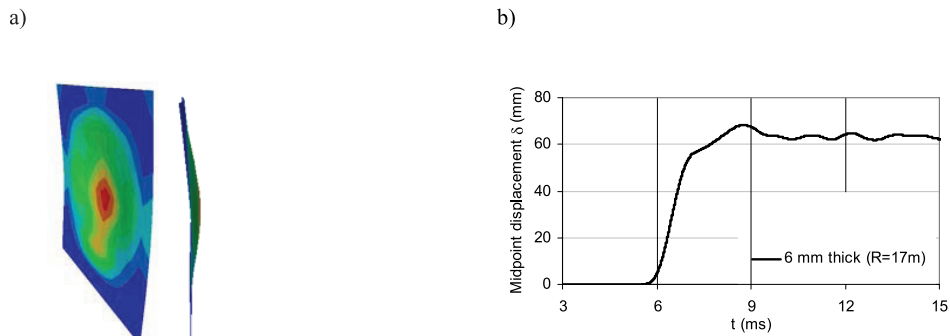
a)   b)

Figure 21. Behaviour of a 6mm steel plate located at 17m from the explosive in blast. 10 a) Plate deformation (plastic work; b) Displacement time history

AKNOWLEDGEMENTS

REFERENCES

1.   Nurick, G.N., Chung Kim Yuen, S., Jacob, N., Verster, W., Bwalya, D. and Vara, A.R., *Response of quadrangular mild-steel plates to large explosive load. Second international conference on design analysis of protective structures (DAPS)*. Nanyang Technological University, 2006, 30–44.

2.   Chung Kim Yuen, S., Nurick, G.N., Verster, W., Jacob, N., Vara, A.R., Balden, V.H. , Bwalya, D., Govender, R.A. and Pittermann, M., Deformation of mild steel plates subjected to large-scale explosions, *Int J Impact Eng*, 2008, 35, 684–703.

3.   Teeling-Smith, R.G. and Nurick, G.N., The deformation and tearing of thin circular plates subjected to impulsive loads, *Int J Impact Eng*, 1991, 11(1), 77-91.

4.   Nurick, G.N. and Shave, G.C., The deformation and tearing of thin square plates subjected to impulsive loads-an experimental study, *Int J Impact Eng*, 1996, 18(1), 99-116.

5.   Nurick, G.N. and Martin, J.B., Deformation of thin plates subjected to impulsive loading—a review. Part I: Theoretical considerations. *Int J Impact Eng*, 1989, 8(2), 159–169.

6.   Nurick, G.N. and Martin, J.B., Deformation of thin plates subjected to impulsive loading—a review. Part II: Experimental studies, *Int J Impact Eng*, 1989, 8(2), 171–186.

7.   Guruprasad, S. and Mukherjee, A., Layered sacrificial claddings under blast loading Part II - Experimental studies, *Int J Impact Eng*, 2000, 24(9), 975-984.

8.   Jacinto, A.C., Ambrosini, R.D. and Danesi, R.F., Experimental and computational analysis of plates under air blast loading, *Int J Impact Eng*, 2001, 25(10), 927–947.

9.   Hanssen, A.G., Enstock, L and Langseth, M. Close-range blast loadin loading of aluminium foam panels, *Int J Impact Eng*, 2002, 27(6), 593–618.

10.   Formby, S.A. and Wharton, R.K., Blast characteristics and TNT equivalence values for some commercial explosives detonated at ground level, *Journal of Hazardous Materials*, 1996, 50, 183-198.

11.   Wharton, R.K., Formby, S.A., and Merrifield, R., Airblast TNT equivalence for a range of commercial blasting explosives, *Journal of Hazardous Materials*, 2000, 79(1-2), 31-39.

12.   Lok, T.S., Response of solid circular ductile cantilever subjected to air-blast, *Private communication*, 2005.

13.   Hirschfelder, J.O., Littler, D.J., and Sheard, H., *Estimated blast pressures from TNT charges of 2 to 10000 tons*, Los Alamos National Laboratory Library, LA Report 316, 3 9338 00350 4049:1-12., 1945.

14. Ambrosini, R.D., Luccioni, B., Danesi, R., Riera, J. and Rocha, M., Size of craters produced by explosive charges on or above the ground surface, *Shock Waves*, 2002, 12(1), 69-78.

15. Ambrosini, R.D. and Luccioni, B., Craters produced by explosions on the soil surface, *J. Applied Mechanics, ASME*, 2006, 73(6), 890-900.

16. Luccioni, B., Ambrosini D., Nurick G.N. and Snyman I. Craters produced by underground explosions, *Computers & Structures*, 2009, 87, 1366-1373.

17. Ambrosini, D and Luccioni, B., Craters produced by large-scale explosions, *Mecánica Computacional, XXVI*, 2008, 1801-1822.

18. Luccioni, B., Ambrosini D. and Danesi, R., Blast load assessment using Hydrocodes, *Eng Struc, 2006*, 28(12), 17361744.

19. Baker, W.E., Cox, P.A., Westine, P.S., Kulesz, J.J. and Strehlow, R.A., *Explosion hazards and evaluation*, Elsevier; 1983.

20. Kinney, G.F. and Graham, K.J., *Explosive Shocks in air*, 2nd ed., Springer Verlag, 1985.

21. Smith, P.D. and Hetherington, J.G., *Blast and Ballistic Loading of Structures*, Butterworth-Heinemann Ltd; 1994.

22. Persson, P. A., Holmberg, R., and Lee, J., *Rock Blasting and Explosives Engineering*, CRC Press, Boca Raton, 1994.

23. Bull, J. W., and Woodford, C. H., Camouflets and their effects on runway supports, *Comput Struct*, 1998, 69(6), 695–706.

24. Henrych, J., *The Dynamics of Explosion and its Use*, Elsevier Scientific Publishing Company, Amsterdam and New York, 1979.

25. Melosh, H. , *Impact Cratering-A Geologic Process*, The Clarendon Press, Oxford University Press, New York, 1989.

26. Iturrioz, I., and Riera, J. D., Numerical study of the effect of explosives on a plane surface, XII Congress on Num. Methods and their Applications, ENIEF 2001, Argentina, 2001.

27. Nurick, G.N., An empirical solution for predicting maximum central deflections of impulsively loaded plates. *International conference on mechanical properties of materials at high rates of strain*, Oxford, 1989, 457 –64.

28. Petes J. Part IV Explosive effects: blast and fragmentation characteristics. *Ann NY Acad Sci 1968*, 152(1):283–316.

29. Cooper PW. Comments on TNT equivalence. In: *Proceedings of the 20th international pyrotechnics seminar, Colorado, USA*, 1994,1–11.

30. AUTODYN, Explicit Software for Non-Linear Dynamics, V11.0, User's Manual, Century Dynamics Inc, 2007.

31. Alia, A. and Souli, M., High explosive simulation using multi-material formulations, *App Thermal Eng*, 2006, 26, 1032-1042

32. Lee, E.L. and Tarver, C.M. Phenomenological model of shock initiation in heterogeneous explosives. *Physics of Fluids*, 2008, 23(12),2362-2372.

33. AUTODYN, Explicit Software for Non-Linear Dynamics, Theory Manual, Revision 4.3, Century Dynamics Inc, 2005.

34. Luccioni, B.M. and Ambrosini D. Evaluating the effect of underground explosions on structures. *Mecánica Computacional*, 2008, 27, 1999-2019.